

# Small-Signal AC Response of an Electrochemical Cell with Completely Blocking Electrodes

J. Ross Macdonald\*

Department of Physics and Astronomy, University of North Carolina, Chapel Hill, North Carolina 27599-3255

## ABSTRACT

An exact solution is presented for the small-signal ac response, in the continuum approximation, of an electrochemical cell, or half-cell, with unsupported electrolyte and completely blocking electrodes. The solution includes the possibility of inner layer capacitance effects, arbitrary mobilities, arbitrary valence numbers, and any degree of charge dissociation. It applies to liquid and solid electrolytes, fused salts, and even intrinsic semiconductors. Numerous complex plane plots are included to demonstrate some of the many types of response possible. The present solution has also been incorporated as a distributed circuit element for use in equivalent circuit fitting using a newly improved complex non-linear least squares fitting program.

The completely blocking (ideally polarized) electrode situation is not uncommon in both liquid and solid electrochemistry areas. But in the former case, *e.g.*, with a mercury electrode, it has been usual to consider only the double layer capacitance in the limit of low frequencies and to assume that it and the solution resistance are essentially frequency independent. Such double layer work has recently been reviewed (1). Complete blocking (no direct current possible) is also observed in the small-signal response of solid electrolytes with nonparent ion electrodes. Further, for both liquids and solids there may be present a thin insulating layer (the inner layer of the electrochemical double layer) between the metallic (or highly conducting liquid) electrode and the material of interest. Such layers may arise uncontrollably from the preparation procedure or, sometimes, may even be included on purpose to ensure complete blocking of all mobile charge carriers present in the material (2). Even in the absence of all such layers, desired or not, there is still present an effective insulating layer (in the absence of a charge transfer reaction) involving charge separation arising from the finite size of mobile ions, a steric effect which ensures that their charge centroids cannot approach an electrode closer than about an ionic radius.

The completely blocking phenomena and frequency response considered in the present work are those appropriate for an unsupported electrolyte. They thus may apply to liquid electrolytes without support, to fused salts, and to most solid-state situations (3), even including intrinsically conducting semiconductors. Although for solids more small-signal ac measurements have been made over a considerable range of frequencies, the domain of impedance spectroscopy (acronym IS) (3), there has been less attention devoted to completely blocking than to partly conducting behavior (4). Another important difference is that when charges of both signs are mobile, the only situation considered here, the ratio of the mobilities of the charges of opposite signs,  $\pi_m$ , may be very large (or very small) for solid electrolytes but is usually fairly close to unity for liquid electrolytes. Thus while one might find a ratio as big as  $10^8$  or more for solids (solid electrolytes, aliovalent single crystals, or even glasses, polymer films, and amorphous materials), a ratio bigger than  $10^2$  would be unusual in the liquid case. In spite of the relative paucity so far of IS measurements for completely blocking situations, much about the basic processes occurring in the material of interest can be learned from such measurements.

Here, some predictions of a general, continuum microscopic theory of such small-signal ac response (5)<sup>1</sup> will be presented to illustrate some of the varied complex plane curve shapes possible. There are too many parameters involved to allow a fully comprehensive study to be presented in a reasonable space for even the completely

blocking response. For the same reason, no detailed frequency response results (*e.g.*, three-dimensional perspective plots (6)) are included. But these omissions are not of great importance here. First, the full, exact, completely blocking solution is summarized in the appendix. More importantly, this solution represents a particular distributed circuit element (DCE), one which may be called the Nernst-Planck element, and is included, along with many other useful DCE's as a part of the author's complex non-linear least squares (CNLS) IS fitting program, LOMFP (7, 8). Since this program, which also includes a great many different equivalent circuits for fitting, is available from the author, it may be used, as the method of choice, in analyzing completely blocking IS data. When data fitting with the current version of LOMFP leads to a good fit of such data, it will also provide direct estimates of either the present primary set of free parameters, or of the microscopic set related to them: parameters such as mobilities, equilibrium bulk concentrations, generation-recombination constants, and so on (5).

The first exact theory for the present situation appeared (9) in 1953. In many later papers, I and my collaborators have generalized it greatly, culminating in the results of Ref. (5). There, the small-signal ac response for both partly and fully blocking electrodes is calculated (but not depicted graphically) for intrinsic and extrinsic conduction situations, for arbitrary dissociation-recombination of mobile and immobile centers, for arbitrary mobilities of the two mobile species present, and for arbitrary valence numbers of these species. Since three and higher body recombinations are not included in the theory, it is only applicable in the incomplete dissociation case for equal valence numbers, but they need not be equal for full dissociation (5).

In a recent paper dealing with polyphenylene-oxide polymer films (10), Glarum and Marshall derive the small-signal ac response of a half-cell containing fully dissociated unsupported material with unity valence numbers and involving a completely blocking electrode. No inner layer effects were included. Thus, this work treated a special case of the considerably more general problem analyzed earlier by the present author, that mentioned in the preceding paragraph. In fact, when the formal results of Ref. (5) are specialized for the Glarum-Marshall simplified situation, they involve the separation out of the geometric capacitance and bulk resistance of the material, include all the rest of the response in an impedance  $Z_s$ , and lead to response equations as simple as those of Glarum and Marshall and fully consistent with them (see Appendix). Both the earlier analytical work of the author (5, 9) and that of Glarum and Marshall (10) apply only to situations where the mobile charge concentration is spatially uniform before the application of a measuring signal, the point of zero charge (pzc) for the electrolyte situation. Since even for the special intrinsic-conduction case, the completely blocking solution of Ref. (5) is considerably more general than that of Ref. (10), it is worthwhile to explore some of the predictions of the former work and to make better known that

\* Electrochemical Society Active Member.

<sup>1</sup> In Ref. (5) the word "generalization" near the top of p. 1626 should be replaced by "generation." The citation of Eq. [14] in the first column of p. 1627 should be Eq. [4]. The  $\Delta_i$  symbols in Table I should be  $\Delta_i^*$ .

the full solution can now be readily included in an equivalent circuit for easy CNLS fitting.

### Discussion of Results

**Circuits and normalization.**—Consider an experimental cell involving two identical plane-parallel electrodes, with the material of experimental interest between them. Then the total impedance,  $Z_T$ , of the unsupported, completely blocking system involves the geometric capacitance,  $C_g$ , in parallel with the series combination of the bulk of solution resistance,  $R_b$ , and the impedance  $Z_s$  defined in the Appendix. Finally, any inner layer capacitance,  $C_i$ , may be taken in series with the above parallel combination. This latter result, although physically plausible for the completely blocking situation, is not immediately obvious. The Ref. (5) analysis uses Chang-Jaffé boundary conditions and thus takes no account of an intrinsic inner layer. But work by Franceschetti and Macdonald (11) shows how an analytic solution using these boundary conditions may be transformed to one which incorporates overpotential-dependent conditions, such as those of Butler and Volmer. Franceschetti (12) has applied this transformation to the present situation, thus accounting properly for the presence of an inner layer in the continuum approximation, and has thereby rigorously justified the presence of its capacitance in series with the rest of the circuit. This capacitance may be readily included as an additional circuit parameter to be determined by CNLS fitting. Here we take  $C_i$  as the combined capacitance of that of the inner layers of each of the two electrodes, taken in series.

In a CNLS fit of completely blocking data there will generally be a maximum of eight parameters involved, although not all of them may be simultaneously free. In addition to  $R_b$ ,  $C_g$ , and possibly  $C_i$ , five further parameters are needed to define  $Z_s$  in the most general case (5). These are, first, a quantity directly associated with the diffuse double layer capacitance,  $M$ , the number of Debye lengths in a half-cell;  $\pi_m$ , the ratio of the mobility of negative charges to that of positive ones;  $\pi_z$ , the ratio of the valence number for negative charges to that for positive ones;  $\Lambda$ , a measure of charge dissociation; and  $\xi$ , the ratio of the recombination relaxation time to the dielectric relaxation time,  $\tau_D = R_b C_g$ . In the simplest case, that considered by Glarum and Marshall, there are only four free parameters to be determined from CNLS fitting:  $R_b$ ,  $C_g$ ,  $M$ , and  $\pi_m$ . Although it might seem from the above that one can only obtain an estimate of the mobility ratio, rather than the individual mobilities, the simultaneous estimation of  $R_b$  and  $C_g$ , along with  $M$  and  $\pi_m$ , allows one to obtain estimates of the separate mobilities and bulk equilibrium concentrations as well since the electrode separation is taken to be known (5).

For convenience in presenting illustrative complex plane plots of some of the completely blocking behavior, several normalizations will be employed. First, all impedances and resistances will be normalized with  $R_b$  and all capacitances with  $C_g$ . Such normalization will be denoted with a subscript "n". Thus,  $Z_{sn} \equiv Z_s/R_b$ . It turns out that for blocking situations like those considered here, as well as for dielectric materials, it is most instructive to present response curves at the complex dielectric or complex capacitance level rather than at the impedance, admittance, or complex modulus level (3, 10). Since the complex capacitance corresponding to an impedance  $Z$  is  $1/(i2\pi\nu Z)$ , the complex capacitance corresponding to the total circuit impedance,  $Z_T$ , is  $C_T = 1/(i2\pi\nu Z_T)$ . As usual, "i" is the positive square root of -1. Let us now introduce the normalized angular frequency  $\Omega \equiv 2\pi\nu\tau_D$ . Then it turns out that  $C_{Tn} = 1/(i\Omega Z_{Tn})$ . This quantity is proportional to the complex dielectric constant, commonly written as  $\epsilon = \epsilon' - i\epsilon''$ . Thus, it is natural to define  $C_{Tn}$  as  $C'_{Tn} - iC''_{Tn}$ .

Our normalization is still incomplete. The low frequency limiting value of  $C_{Tn}$  is  $C_{Tn0} = C'_{Tn0} = r \equiv (M)ctnh(M)$ , essentially equal to  $M$  for  $M > 3$  and independent of generation-recombination effects except for their influence on the value of  $M$  (see later discussion). Since the minimum value of  $C_T$  is its high frequency limiting value of  $C_g$ , the minimum value of  $C_{Tn}$  is unity. In order that complex plane

plots of the complex capacitance may all be plotted in the region from 0 to 1, we need to normalize  $C_{Tn}$  with  $r$ ; such normalization will be denoted with a subscript "N". Thus  $C_{TN} \equiv C_{Tn}/r$ . The high frequency limiting value of the real part of this quantity is then  $1/r$  and its low frequency limiting value is unity.

The above results apply when the effects of any inner layer are negligible. Since this may not always be the case, let us introduce further normalization which will ensure that the maximum value of  $C'_{TN}$  is still unity for any value of  $C_i$ , itself taken frequency independent. Define  $C_{IN} \equiv C_{In}/r$  and rename  $C_{TN}$  in the absence of inner layer effects to  $C_{BN}$ ; it is this quantity, with "n" normalization, which is calculated in the Appendix. Then, finally, we may write  $C_{TN} = [(1 + C_{IN})/(C_{BN} + C_{IN})]C_{BN}$ . This is the expression plotted in the present graphs. Clearly it reduces to  $C_{BN}$  for  $C_i \gg C_B$ , often the situation of interest. Note that  $C_{IN}$  is just the ratio of the combined inner layer capacitances to the low frequency limiting value of the completely blocking (diffuse double layer) capacitance.

**Graphical results.**—We shall first show some possible curve shapes for the completely dissociated case without inner layer effects. Unless otherwise noted,  $C_i$  will be taken as infinite hereafter. Figure 1 indicates how the complex plane  $C_{TN}$  shape depends on  $\pi_m$  when  $\pi_z = 1$ . This is the only situation considered by Glarum and Marshall in their interesting work, and the present results are directly comparable to theirs and essentially the same. Here frequency increases from right to left so the right bottom corner is the zero-frequency point. The slight irregularities in some of the curves herein are artifacts which arise from the machine plotting procedure used. All curves involve about 100 points, with equal steps of  $\log(\Omega)$ , and points are connected by straight lines.

The curves of Fig. 1 and other similar results allow several conclusions to be drawn. First, when the mobilities are equal and thus  $\pi_m = 1$ , one obtains a curve which is usually experimentally indistinguishable from a full semicircle (single-time constant Debye response). But see the discussion below. The normalized response is entirely independent of generation-recombination conditions. The simple analytical expression for this  $\pi_m = 1$  response is included in the Appendix.

As  $\pi_m$  increases from unity towards  $M$ , the  $C_{TN}$  curve becomes distorted, as in Fig. 1, and for  $\pi_m \gg M$  it divides into two distinct parts, a high frequency semicircle and a low frequency arc reminiscent of diffusion effects. This arc is, in fact, associated with diffusion processes arising from the very large difference in the mobilities. When  $\pi_m \gg M \gg 1$ , the semicircle and the arc are well separated in frequency. For  $\pi_z = 1$ , it turns out that the maximum values of  $Im(C_{TN})$  are  $2^{-3/2}$  and about 0.0743, occurring at  $\Omega$  values of  $2^{1/2}/M$  and  $(e\pi_m)^{-1}$ , respectively. Incidentally, for  $\pi_z = 1$  but not otherwise, all the present results would have been obtained for  $\pi_m$  values taken as the inverses of those shown, just as required from symmetry.

When inner layer effects are negligible and exact Debye behavior is observed, the diffuse double layer capacitance,

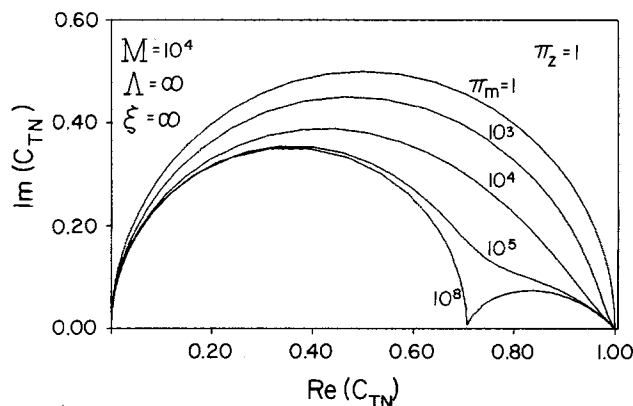


Fig. 1. Complex plane plot of  $C_{TN}$  for full dissociation and unit valence number ratio,  $\pi_z$ . Dependence on mobility ratio,  $\pi_m$ , for  $M = 10^4$ .

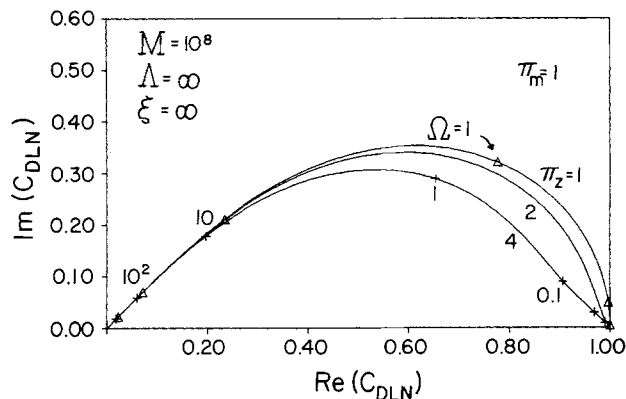
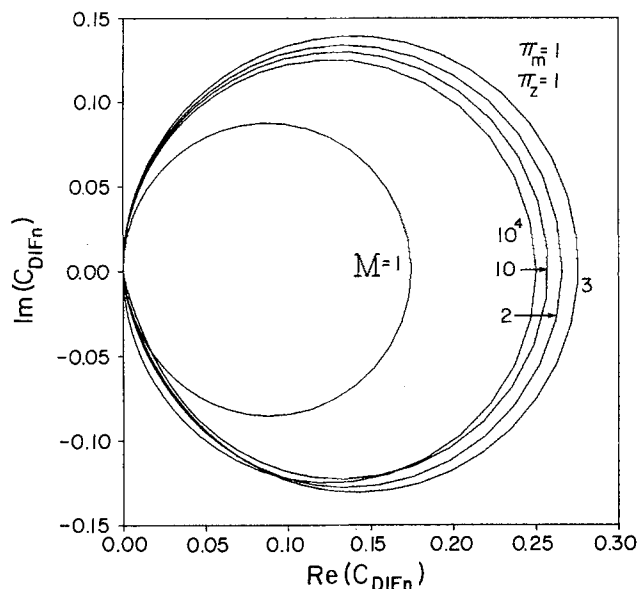


Fig. 2. (a, left) Complex plane plot of  $C_{DIFn}$ , a measure of the deviation from Debye response, for  $\pi_m = \pi_z = 1$  and several  $M$  values. (b, right) Complex plane plot of  $C_{DLN}$  at high normalized frequencies for  $\pi_m = 1$  and  $\pi_z = 1, 2$ , and  $4$ .

$C_{DL}$ , is frequency independent. But the present  $\pi_m = \pi_z = 1$  exact solution yields response close to but not exactly the same as Debye response. It is thus of interest to examine the difference and the corresponding frequency dependence of  $C_{DL}$ . It turns out that the complex plane curve shape of the deviation,  $C_{DIF}$ , of the present  $\pi_m = 1$  curve from an exact Debye curve with the same low and high frequency limiting values is essentially independent of  $M$  for large  $M$ . Therefore, we shall use "n" normalization for  $C_{DIF}$ .

Figure 2a presents both large and small  $M$  complex plane plots of  $C_{DIFn} \equiv C'_{DIFn} + iC''_{DIFn}$ , defined analytically in the Appendix. Here frequency increases clockwise. For large  $M$ , the deviation curve is a perfect circle with maximum values of  $\text{Re}(C_{DIFn})$ , 0.25, occurring at  $\Omega M = 1$ . Correspondingly, the maximum values of  $|\text{Im}(C_{DIFn})|$  occur at  $\Omega M = 2^{1/2} - 1$  and its inverse,  $2^{1/2} + 1$ . The curves are not entirely symmetric for small  $M$ , and  $M$  near 4 yields the maximum value of  $\text{Re}(C_{DIFn})$ . Since these results show that the deviations between the exact  $\pi_m = 1C_T$  curve and the matching Debye curve are always a small fraction of  $C_g$ , the Debye approximation is adequate except for small  $M$ , where the maximum value of  $\text{Re}(C_T)$  will only be slightly larger than  $C_g$  [see, e.g., Fig. 4a].

Figure 2b shows some  $\pi_m = 1$  complex plane curves for  $C_{DLN} = 1/[i\Omega Z_{sn}(r-1)] = C'_{DLN} - iC''_{DLN}$ . Note that here "N" normalization involves the low frequency limiting value of  $C_{DLn}$ ,  $r-1$ , rather than  $r$ . The difference is negligible for large  $M$  but becomes important when  $M$  is small. Curves for different values of  $M$  are not included because with the present normalization even  $M = 0.3$  results are very close in shape to those for large  $M$ . The present  $\pi_z = 1$  result is a typical finite length diffusion curve, involving constant phase element response at high frequencies (3, 4). The points marked on the  $\pi_z = 1$  and 4 curves are included to give some idea of frequency dependence. Notice that the  $C_{DLN}$  curve for  $\pi_z = 1$  does not begin to exhibit appreciable frequency dependence until  $\Omega$  is larger than 0.01, often a higher frequency region than convenient to measure, but the  $\pi_z = 4$  curve shows such departure from the low frequency limiting value when  $\Omega$  is as small as  $10^{-3}$ . The  $\pi_z = 1$  curve involves a peak value of  $C''_{DL}$  of about  $0.35(r-1)C_g$ , much larger than  $C_g$  for large  $r$  and  $M$  but only about a tenth of  $C_g$  for  $M = 1$ . Further, the value of  $\Omega$  at the peak is about 1.6 for  $M \gg 1$  but is about 14 for  $M = 1$  and about 140 for  $M = 0.3$ , much above the ordinary IS frequency measurement range for usual values of  $\tau_D$ .

What is the interpretation of these  $\pi_m = 1$  results? It is that only for  $M$  of the order of unity is it likely that  $C_{DL}$  can be adequately determined from IS data for the present high end of the  $\Omega$  range. Since we can write, in terms of complex capacitances,  $C_{DLn} = (C_{Tn} - 1)/[1 - i\Omega(C_{Tn} - 1)]$ , it

is clear that when  $|C_{Tn}|$  is very nearly unity, as it is for large  $M$  when  $\Omega > 0.01$ , an accurate value of  $C_{DLn}$  cannot be calculated from even excellent data in this region. Rewriting the above equation as  $C_{Tn} = 1 + [i\Omega + C_{DLn}^{-1}]^{-1}$ , one sees that only when  $|C_{DLn}^{-1}|$  is of the order of unity or greater, as it will be for small  $M$  in this high frequency range, or for large  $M$  for  $\Omega \ll 0.01$ , will  $C_{DLn}$  contribute appreciably to  $C_{Tn}$ . Of course when  $C_T$  response is not close to Debye response,  $C_{DL}$  will vary appreciably with frequency and is of less interest compared to the frequency independent primary parameters of the completely blocking solution.

Figure 3 shows the effect of  $\pi_z$  variation on two of the curves appearing in Fig. 1. When the more mobile charge also has the largest valence number, Fig 3a shows that the curves again approach Debye behavior for large  $\pi_z$ . Note the dependence of the cusp value of  $\text{Re}(C_{Tn})$  for Fig. 3b on  $\pi_z$ . For  $\pi_z = 1$  it approaches  $1/2^{1/2}$  for large  $M$ .

Figure 4a indicates how curve shape depends on  $M$  for the  $\pi_m = 10^8$  curve of Fig. 1. Note that for  $M \gg \pi_m$ , Debye behavior is again approached. The present "N" normalization allows all these curves to be presented on the same scale. Had "n" normalization been used, the  $M = 1$  curve would have had a  $\text{Re}(C_{Tn})$  intercept of unity at high frequencies and a low frequency intercept of only  $r = \text{ctnh}(1) = 1.313$ . Figure 4b shows the effect of a series capacitance,  $C_{IN}$ , on one of the curves of Fig. 1. For small  $C_{IN}$ , Debye behavior is approached once more. But note that for  $C_{IN} \ll 1$ , the high frequency limiting value of  $\text{Re}(C_{Tn})$  approaches  $1/(1 + rC_{IN})$ . Thus for  $C_{IN} = 1/r$ , this value is 0.5.

Let us conclude by considering partial dissociation behavior. Let  $D$  denote the dissociation ratio, a quantity given (5) by  $1/(1 + \Lambda^{-1})$ . Thus  $D = 1(\Lambda = \infty)$  indicates full dissociation, and  $D = 0.5$  for  $\Lambda = 1$ . For this value of  $\Lambda$ , Fig. 5a show how curve shape depends on the relaxation time ratio  $\xi$  for  $\pi_m = 10^8$ . Note that three individual arcs are beginning to appear for the  $\xi = 10^6$  curve. Figure 5b alternatively keeps  $\xi$  fixed at 100 and indicates the effect of varying  $\Lambda$ . For small dissociation, Debye behavior is again approached. In Fig. 6, I have shown just the low frequency part of the  $\xi = 10^6$  curve of Fig. 5a. The curves of Fig. 6a and b are included to give the reader some idea of how the low frequency arc itself can split into two diffusion-related arcs as the dissociation increases and then meld back to a single arc as full dissociation is approached.

The curves presented so far give only a very incomplete picture of all the response shapes possible for the completely blocking situation. Further, in the real world, the parameters are not all independent. The curves of Fig. 7 are included to provide some idea of response with interdependent parameters. Let us allow the equilibrium bulk

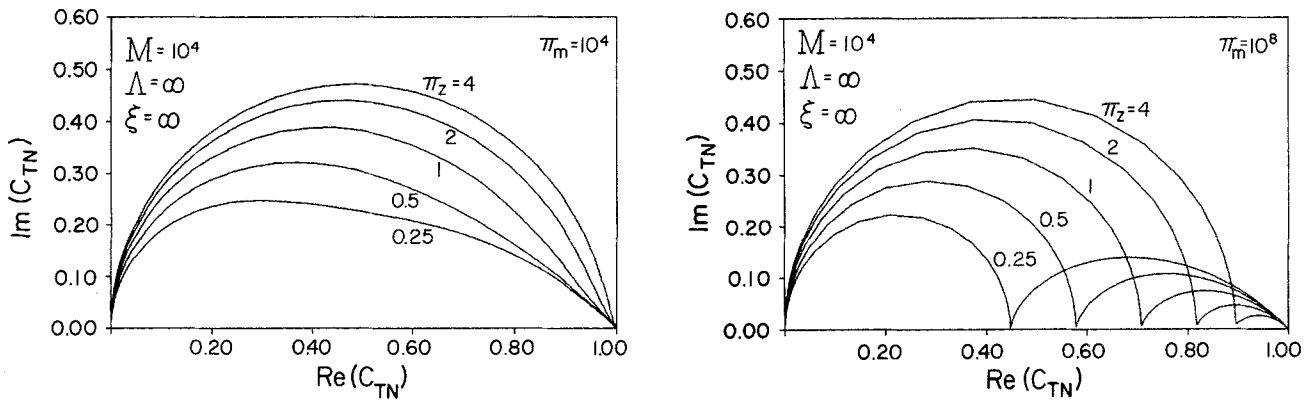


Fig. 3. Complex plane plot of  $C_{TN}$  with  $M = 10^4$  showing dependence on  $\pi_z$  for (a, left)  $\pi_m = 10^4$  and (b, right)  $\pi_m = 10^8$

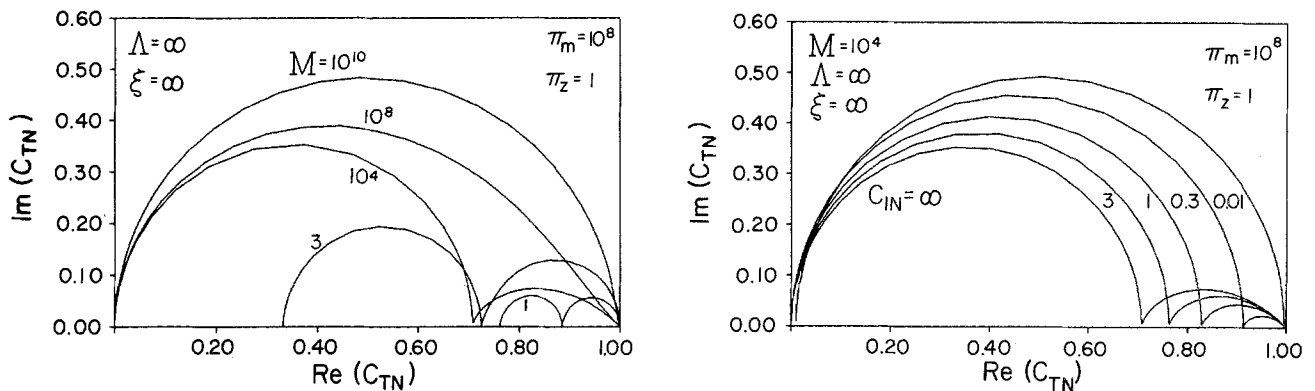


Fig. 4. Complex plane plot of  $C_{TN}$  for  $\pi_m = 10^8$  and  $\pi_z = 1$  showing (a, left) dependence on  $M$ , and (b, right) dependence on the series capacitance ratio,  $C_{IN}$ .

concentration to vary, so that  $D$  correspondingly varies. We shall take  $D$  values of 1, 0.5,  $10^{-2}$ ,  $10^{-3}$ , and  $10^{-4}$ . For  $D = 1$ , we take  $M = 300$ ,  $\xi = 10^4$ ,  $\pi_m = 10^4$ , and  $\pi_z = 1$ . These last two quantities will be taken independent of  $D$ , but  $M$  is proportional to  $D^{1/2}$  and  $\xi$  to  $D$  for the present situation. Only the  $M$  values are shown on the graph but  $\Lambda$  and  $\xi$  vary as above with  $M$  and  $D$ . The shapes obtained are interesting, but different ones would have appeared had the initial value of  $\xi$ , for example, been different.

Since we cannot hope to illustrate even a fraction of the possible behavior here, it is useful that the full solution is available for CNLS fitting, but even such fitting may not allow full discrimination between the various special conditions that can lead to essentially Debye behavior. In such limiting cases, other independent information will usually be required to elucidate the response fully. For example, if  $C_{TN} \ll 1$  so that  $C_I$  dominates the capacitive response, the complex-capacitance plane response of  $C_T$  will be a Debye curve arising just from  $R_b$  and  $C_I$  in series. In this case, the overall response will show little dependence on

an applied static potential since  $C_I$  should be field independent or nearly so, while  $C_{DL}$  depends strongly on static potential (1, 3, 4, 13). Such potential independence of  $C_T$  was, in fact, found by Glarum and Marshall (10) for their measurements on a completely blocking system.

It should be emphasized that the present results only illustrate the completely blocking behavior of bulk material, particularly that present when  $\pi_m$  is very different from unity and thus the full response extends over a very wide range of frequencies. The present response possibilities take no account of possible electrode roughness and thus best apply for liquid metal or, perhaps, concentrated electrolyte electrodes. But solid metal electrodes always exhibit some surface roughness, adding an interface impedance to the present  $Z_s$  response. Such an impedance may also be significant over a wide range of frequency, possibly overlapping the bulk response range or even occurring below it. It is thus important to understand the bulk response so it can be separated from the interface impedance when one is interested in studying one or the

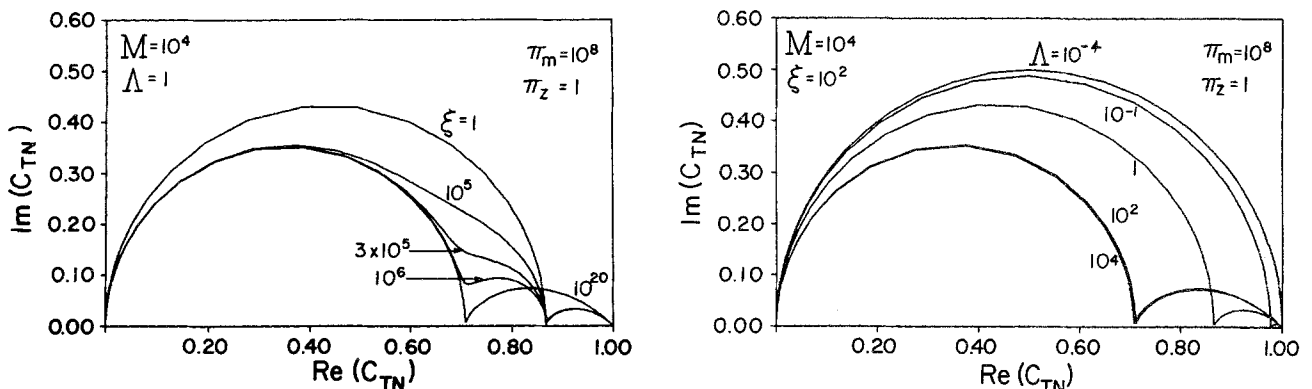


Fig. 5. Complex plane plot of  $C_{TN}$  under partly dissociated conditions for  $M = 10^4$ ,  $\pi_m = 10^8$ , and  $\pi_z = 1$  with (a, left)  $\Lambda = 1$  and  $\xi$  variable, and (b, right)  $\xi = 10^2$  and  $\Lambda$  variable.

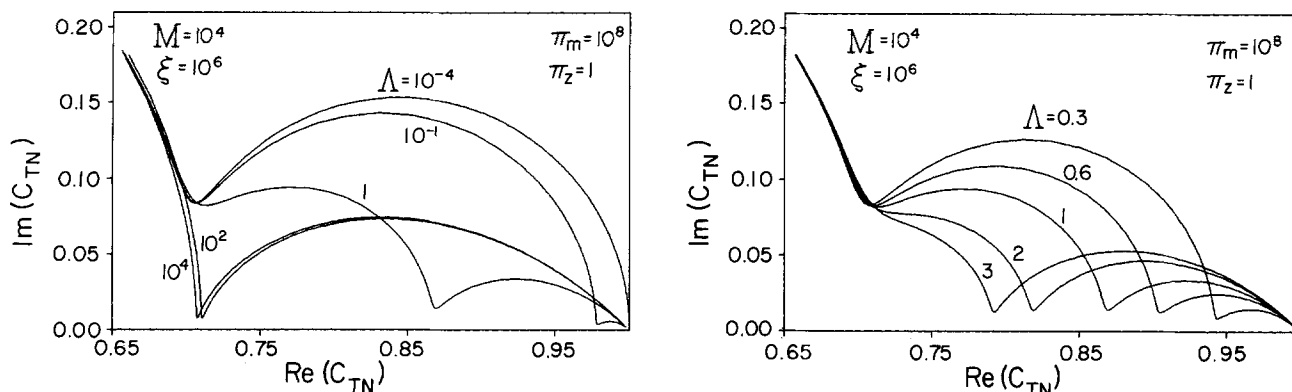


Fig. 6. Complex plane plot of low frequency part of  $C_{TN}$  under partly dissociated conditions for  $M = 10^4$ ,  $\pi_m = 10^8$ , and  $\pi_z = 1$ , with  $\xi = 10^6$  and  $\Lambda$  variable.

other or both of these contributions. The interface impedance is usually found to exhibit constant phase angle (CPE) response (3, 4, 14) over a wide frequency span. Such response appears in many small-signal response theories (15) and can arise from various quite different physical sources. Recently, various different fractal-related theories of such interface CPE response have been proposed (16), but currently unpublished work of Bates and his collaborators (17) strongly suggests that although the response is indeed associated with surface roughness, it is unrelated to the fractal dimension of the surface. Although the combination of bulk and interface effects can lead to more complicated complex plane curves than those illustrated, I shall not show any such results here. Data possibly arising from the combination of both effects should be plotted in both the impedance (and possibly log impedance) and complex capacitance planes and analyzed using CNLS.

Although the present results were derived for a system with two identical electrodes, common for solid materials, they also apply, in their present normalized form, to half-cell response, the usual situation for liquid electrolytes. In the latter case, actual impedance and capacitance values may be obtained from the normalized expressions of the appendix by using normalization values which take account of the presence of one rather than two electrodes. Because of the symmetry of the system with two identical electrodes, it may be considered to consist of two identical half-cells in series, with the center of the material, the joining point of the half-cells, a unique point where bulk concentrations retain their equilibrium values and remain undisturbed by the applied ac potential.

As already mentioned, the present graphical results represent only a small part of all the potential responses which can arise from possible variations in mobility and valence ratios, generation-recombination, geometric effects, inner layer capacitance, and electrode roughness. Nevertheless, they may be of some immediate diagnostic value. When the system being investigated is completely blocking, or thought to be so, one should first consider the response in the complex capacitance plane by forming and

plotting  $C_T = 1/(i2\pi\nu Z_T) \equiv Y_T/(i\omega) \equiv C'_T - iC''_T$ . The results, as functions of such external variables as temperature and/or electrode separation, may then be compared qualitatively with the curve shapes presented herein. If similar shapes are found, one should then be able to obtain semi-quantitative estimates of such quantities as  $M$ ,  $\pi_m$ , and possibly even  $\pi_z$  and the recombination parameters. These estimates could then be employed as initial parameter values for use in subsequent CNLS fitting of the data.

It is worth emphasizing that it is always very desirable to go beyond qualitative comparisons and carry out full CNLS fitting of the data. Such fitting is generally quite insensitive and forgiving to the initial parameter guesses and can usually converge to a good fit even when such guesses are orders of magnitude from their final converged values. Thus, such fitting is often useful even when no qualitative agreement can be found between the complex capacitance plane response of the data and any of the present theoretical responses. When a good fit has been obtained, one can immediately identify and quantify the various physico-chemical processes contributing to the overall response. The CNLS program available from the author allows one to fit an equivalent circuit which may contain geometric capacitance, bulk, resistance, a specific Nernst-Planck blocking element, and possible electrode roughness contributions to the overall impedance. In favorable cases, which usually means having reasonably accurate data extending over many decades of frequency, all these processes, and the microscopic quantities associated with them, may be identified and quantified using CNLS fitting.

### Acknowledgments

I much appreciate the helpful comments of Dr. D. R. Franceschetti and the support of the U.S. Army Research Office.

Manuscript submitted Sept. 9, 1987; revised manuscript received Nov. 16, 1987.

The University of North Carolina, Chapel Hill, assisted in meeting the publication costs of this article.

### APPENDIX

The expression for  $Z_{sn}$  given in Eq. [32] of Ref. (5) for the unsupported, completely blocking situation becomes, in the absence of extrinsic conduction

$$Z_{sn} = (\psi/i\Omega)[F_1\gamma_1 - F_2\gamma_2]/[F_1 - F_2]t_1t_2 + F_1t_2 - F_2t_1 \quad [A-1]$$

Let  $j = 1, 2$ . Then  $F_j \equiv \vartheta_j^2 - \psi$ ,  $\gamma_j \equiv (M\vartheta_j^2)ctnh(M\vartheta_j^2)$ , and  $t_j \equiv \gamma_j - 1$ . Here  $\psi \equiv 1 + i\Omega$ , and the  $\vartheta_j^2$ 's are the solutions of a quadratic eigenvalue equation; see below for full definitions. When the identity  $[(F_1 - F_2)t_1t_2 + F_1t_2 - F_2t_1] \equiv [F_1\gamma_1t_2 - F_2t_1\gamma_2]$  is substituted into Eq. [A-1], one obtains  $Z_{sn}$  in its simplest form

$$Z_{sn} = (\psi/i\Omega)[F_1\gamma_1 - F_2\gamma_2]/[F_1\gamma_1t_2 - F_2t_1\gamma_2] \quad [A-1']$$

Now since

$$Y_{TN} = i\Omega + [1 + Z_{sn}]^{-1} \quad [A-2]$$

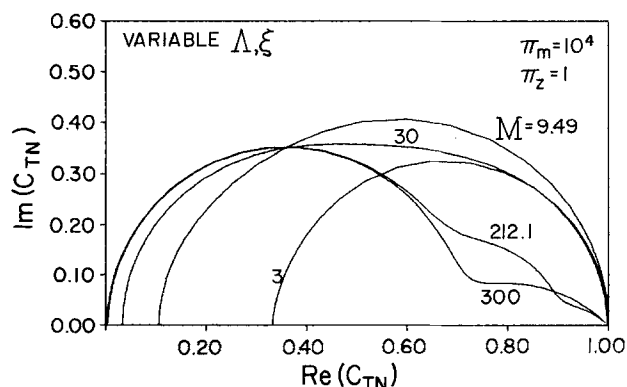


Fig. 7. Complex plane plot of  $C_{TN}$  under variable, partly dissociated conditions for  $\pi_m = 10^4$ ,  $\pi_z = 1$ , and  $M$ ,  $\xi$ , and  $\Lambda$  covarying (see text).

and

$$C_{Tn} \equiv Y_{Tn}/i\Omega$$

we obtain

$$C_{Tn} = 1 + [i\Omega(1 + Z_{sn})]^{-1} \quad [A-3]$$

appropriate when inner layer series capacitance effects are negligible. Equations [A-1'] and [A-3] may be shown to be fully consistent with the analytic results of Ref. (10) when  $\pi_z = 1$  and  $\Lambda$  and  $\xi$  are infinite.

Now Eq. [A-1'] simplifies greatly when  $\pi_m$  and  $\pi_z$  are both unity (5). Then (see below),  $\delta_1^2 = \psi$ ,  $\delta_2^2 = i\Omega(1 + f)$ , and  $F_1 = 0$ . The quantity "f" is defined below. One finds  $Z_{sn} = \psi/[i\Omega t_1]$ , where here  $t_1 \equiv (M\psi)ctnh(M\psi) - 1$ . It follows that

$$C_{Tn} = C_{T1n} \equiv \psi\gamma_1/[1 + i\Omega\gamma_1] \quad [A-4]$$

Now since the low and high frequency limiting values of  $C_{Tn}$  are  $r \equiv (M)ctnh(M)$  and unity, respectively, normalized Debye response which best approximates the Eq. (A-4) response will be of the form

$$C_{D_{yn}} = 1 + (r - 1)/[1 + i\Omega r] \quad [A-5]$$

Then

$$C_{DIFn} \equiv C_{T1n} - C_{D_{yn}} \quad [A-6]$$

a measure of the departure of  $C_{T1n}$  from Debye behavior.

Although all the quantities necessary to calculate  $C_{Tn}$  are defined in Ref. (5), their definitions are given below for completeness. But relations between the present parameters, such as  $R_b$  and  $\Lambda$ , and microscopic quantities will not be repeated here.

Let  $\epsilon_1 \equiv (1 + \pi_m)^{-1}$ ,  $\epsilon_2 \equiv (1 + \pi_m^{-1})^{-1}$ ,  $\delta_1 \equiv (1 + \pi_z)^{-1}$ , and  $\delta_2 \equiv (1 + \pi_z^{-1})^{-1}$ . Define  $\lambda_j \equiv \delta_j/\epsilon_j$  and take  $b \equiv \lambda_1\lambda_2$ ,  $d \equiv \lambda_1 + \lambda_2$ , and  $f \equiv 2b[\Lambda + i\Omega\xi]$ . Then if  $A \equiv 4i\Omega\psi(b + f)$  and  $B \equiv 1 + i\Omega(d + f)$ ,  $\delta_2^2$  is best expressed as (5)

$$\delta_2^2 = (A/4B)[1 + A/B + (B^2 - A)^{1/2}]^2 \quad [A-7]$$

and

$$\delta_1^2 = B - \delta_2^2 \quad [A-8]$$

## REFERENCES

1. J. R. Macdonald, *J. Electroanal. Chem. Interfacial Electrochem.*, **223**, 1 (1987).
2. J. R. Macdonald, *J. Chem. Phys.*, **30**, 806 (1959).
3. "Impedance Spectroscopy—Emphasizing Solid Materials and Systems," J. R. Macdonald, Editor, John Wiley & Sons, Inc., New York (1987).
4. J. R. Macdonald, *J. Electroanal. Chem. Interfacial Electrochem.*, **223**, 25 (1987).
5. J. R. Macdonald and D. R. Franceschetti, *J. Chem. Phys.*, **68**, 1614 (1978).
6. J. R. Macdonald, J. Schoonman, and A. P. Lehen, *Solid State Ionics*, **5**, 137 (1981).
7. J. R. Macdonald, J. Schoonman, and A. P. Lehen, *J. Electroanal. Chem. Interfacial Electrochem.*, **77**, 131 (1982).
8. J. R. Macdonald and L. D. Potter, Jr., *Solid State Ionics*, **23**, 61 (1987).
9. J. R. Macdonald, *Phys. Rev.*, **92**, 4 (1953).
10. S. H. Glarum and J. H. Marshall, *This Journal*, **132**, 2939 (1985).
11. D. R. Franceschetti and J. R. Macdonald, *J. Electroanal. Chem. Interfacial Electrochem.*, **82**, 271 (1977).
12. D. R. Franceschetti, Private communication.
13. D. R. Franceschetti and J. R. Macdonald, *J. Electroanal. Chem. Interfacial Electrochem.*, **100**, 583 (1979).
14. J. R. Macdonald, *Solid State Ionics*, **13**, 147 (1984).
15. J. R. Macdonald, *J. Appl. Phys./Appl. Phys. Revs.*, **15**, R51 (1987).
16. S. H. Liu, *Phys. Rev. Lett.*, **55**, 529 (1985); T. Pajkossy and L. Nyikos, *This Journal*, **133**, 2061 (1986); T. Kaplan, L. J. Gray, and S. H. Liu, *Phys. Rev. B*, **35**, 5379 (1987).
17. J. B. Bates, Personal communication; submitted to *Phys. Rev. Lett.*

## Measurement of Diffusion Coefficients by DC and EHD Electrochemical Methods

Baldwin Robertson

Chemical Process Metrology Division, National Bureau of Standards, Gaithersburg, Maryland 20899

Bernard Tribollet and Claude Deslouis

Laboratoire Propre no. 15 du CNRS, Physique des Liquides et Electrochimie, Université Pierre et Marie Curie, 75230 Paris Cedex 05, France

## ABSTRACT

The electrohydrodynamic (EHD) method of measuring the Schmidt number is compared carefully with the dc method using a rotating disk electrode. Ferricyanide and ferrocyanide ions in 1M potassium chloride are used for the comparison. The best agreement between the two methods occurs when the EHD measurement is done at a low disk velocity.

The measurement of a molecular diffusion coefficient  $D$  by electrochemical techniques is generally done with a rotating disk electrode in order to control the convection of the electrolyte and hence the mass transfer of the diffusing species. The diffusion coefficient obtained in this way has the same definition as that obtained from the spreading of a dye or of a radiotracer in a capillary.

The equation linking the mass-transfer limited current of an electrochemical redox reaction to the angular velocity of the disk has been derived by Levich (1), improved by others (2-4), and reviewed by several authors (5-7). However, using this technique for measuring the diffusion coefficient requires an accurate knowledge of the electrode area  $A$ , the bulk concentration  $C$  of the diffusing species, the number  $n$  of electrons transferred in the reaction

used, and the kinematic viscosity  $\nu$  of the electrolyte. Errors in measuring these quantities can cause a substantial error in determining  $D$ .

Transient methods partially overcome this disadvantage and measure the Schmidt number  $Sc = \nu/D$  directly so that the only unknown parameter is the kinematic viscosity. Among these methods are the ac electrochemical impedance method and the electrohydrodynamic (EHD) method.

With the ac electrochemical impedance method (8-11), the electrode potential is modulated sinusoidally at constant disk speed, and the resulting sinusoidal electrochemical current is measured as a function of modulation frequency. The Schmidt number is obtained from the frequency dependence of the impedance. In order to ob-